The EMBO Journal (2013) 32, 1115–1127
www.embojournal.org

OPEN ACCESS SOURCE DATA TRANSPARENT PROCESS

THE EMBO JOURNAL

The rough endoplasmatic reticulum is a central nucleation site of siRNA-mediated RNA silencing

Lukas Stalder[1,4,*], Wolf Heusermann[1], Lena Sokol[1], Dominic Trojer[1], Joel Wirz[1], Justin Hean[1,5], Anja Fritzsche[1], Florian Aeschimann[1,2], Vera Pfanzagl[1], Pascal Basselet[1], Jan Weiler[1], Martin Hintersteiner[1], David V Morrissey[3] and Nicole C Meisner-Kober[1,*]

[1]Novartis Institutes for Biomedical Research, NIBR Biologics Center, RNAi Therapeutics, Basel, Switzerland, [2]Friedrich Miescher Institute, Basel, Switzerland and [3]Novartis Institutes for Biomedical Research, NIBR Biologics Center, RNAi Therapeutics, Cambridge, MA, USA

Despite progress in mechanistic understanding of the RNA interference (RNAi) pathways, the subcellular sites of RNA silencing remain under debate. Here we show that loading of lipid-transfected siRNAs and endogenous microRNAs (miRNA) into RISC (RNA-induced silencing complexes), encounter of the target mRNA, and Ago2-mediated mRNA slicing in mammalian cells are nucleated at the rough endoplasmic reticulum (rER). Although the major RNAi pathway proteins are found in most subcellular compartments, the miRNA- and siRNA-loaded Ago2 populations co-sediment almost exclusively with the rER membranes, together with the RISC loading complex (RLC) factors Dicer, TAR RNA binding protein (TRBP) and protein activator of the interferon-induced protein kinase (PACT). Fractionation and membrane co-immune precipitations further confirm that siRNA-loaded Ago2 physically associates with the cytosolic side of the rER membrane. Additionally, RLC-associated double-stranded siRNA, diagnostic of RISC loading, and RISC-mediated mRNA cleavage products exclusively co-sediment with rER. Finally, we identify TRBP and PACT as key factors anchoring RISC to ER membranes in an RNA-independent manner. Together, our findings demonstrate that the outer rER membrane is a central nucleation site of siRNA-mediated RNA silencing.

The EMBO Journal (2013) **32,** 1115–1127. doi:10.1038/emboj.2013.52; Published online 19 March 2013
Subject Categories: membranes & transport; RNA
Keywords: argonaute 2; microRNA; RNA interference; rough endoplasmatic reticulum; siRNA localization

*Corresponding authors. L Stalder or NC Meisner-Kober, Novartis Institutes for Biomedical Research, Developmental and Molecular Pathways, Novartis Campus, Fabrikstrasse 22.2.023, Basel 4000, Switzerland. Tel.: +41 76 3981721; E-mail: lukas.stalder@sakk.ch or Tel.: +41 79 4099798; Fax: +41 61 6967470;
E-mail: nicole.meisner-kober@novartis.com
[4]Present address: Swiss Group for Clinical Cancer Research, Bern, Switzerland.
[5]Present address: University of the Witwatersrand Medical School, School of Pathology, Johannesburg, South Africa.

Received: 2 July 2012; accepted: 31 January 2013; published online: 19 March 2013

Introduction

Since the discovery of RNA interference (RNAi), the interest in small RNAs as both therapeutic targets and agents has been growing rapidly. The effective and safe delivery of small RNA therapeutics into cells remains one of the biggest challenges, which is partially linked to the still incomplete picture of the intracellular sites of endogenous RNA silencing. Small-interfering RNAs (siRNAs) and microRNAs (miRNAs) exhibit their functions once they are loaded into RNA induced silencing complexes (RISCs) (Carthew and Sontheimer, 2009). Proteins from the Argonaute (Ago) family are the core of RISCs, and Argonaute2 (Ago2) is the only of the four mammalian Ago proteins with the ability to slice the target mRNA by endonucleolytic cleavage (Liu *et al*, 2004; Meister *et al*, 2004). Although Ago2 can bind single-stranded siRNAs *in vitro* (Rivas *et al*, 2005), endogenous loading of double-stranded small RNAs is thought to require the RISC loading machinery (Liu *et al*, 2004; Yoda *et al*, 2010). The canonical, minimal human RISC loading complex (RLC) comprises Ago2, Dicer and TAR RNA binding protein (TRBP) (Gregory *et al*, 2005; Maniataki and Mourelatos, 2005; MacRae *et al*, 2008; Noland *et al*, 2011). This triad of proteins is capable of binding and processing dsRNA into 21–23nt siRNAs or miRNAs, loading of Ago2 and removing the passenger strand (MacRae *et al*, 2008). As Dicer knockout mouse embryonic stem (ES) cells—while devoid of mature miRNAs—are however proficient of siRNA-mediated gene silencing (Kanellopoulou *et al*, 2005), it has been suggested that this canoncial mode of RISC loading can be bypassed by other mechanisms, one of them involving the Heat shock cognate 70 (Hsc70) and Heat shock protein 90 (Hsp90) chaperones (Miyoshi *et al*, 2005; Iki *et al*, 2010; Iwasaki *et al*, 2010; Johnston *et al*, 2010; Miyoshi *et al*, 2010). Once Ago2 is loaded with the double-stranded siRNA, only one strand (guide) is retained and the other strand (passenger) gets removed and degraded (Matranga *et al*, 2005; Rand *et al*, 2005; Leuschner *et al*, 2006; Miyoshi *et al*, 2010), which can be facilitated by a complex consisting of TRAX and translin (C3PO, component 3 promoter of RISC) (Liu *et al*, 2009; Ye *et al*, 2011).

The specific subcellular sites of the RISC loading, target association and mRNA silencing steps remain under debate. Ago2, miRNAs and target mRNAs that are targeted for translational inhibition have been found to localize to P-bodies (Liu *et al*, 2005; Pillai *et al*, 2005; Jagannath and Wood, 2009), and it has been suggested that miRNAs and RNAi proteins guide their target mRNAs to P-bodies (Jakymiw *et al*, 2005; Pillai *et al*, 2005; Eulalio *et al*, 2007b). However, microscopically visible P-bodies do not seem to be required for RNAi (Chu and Rana, 2006; Eulalio *et al*, 2007b), but have been proposed to be rather a consequence than a cause of silencing (Eulalio *et al*, 2007a, 2007b). Moreover, siRNAs have been found to localize to P-bodies as double strands in an at least partially Ago2-

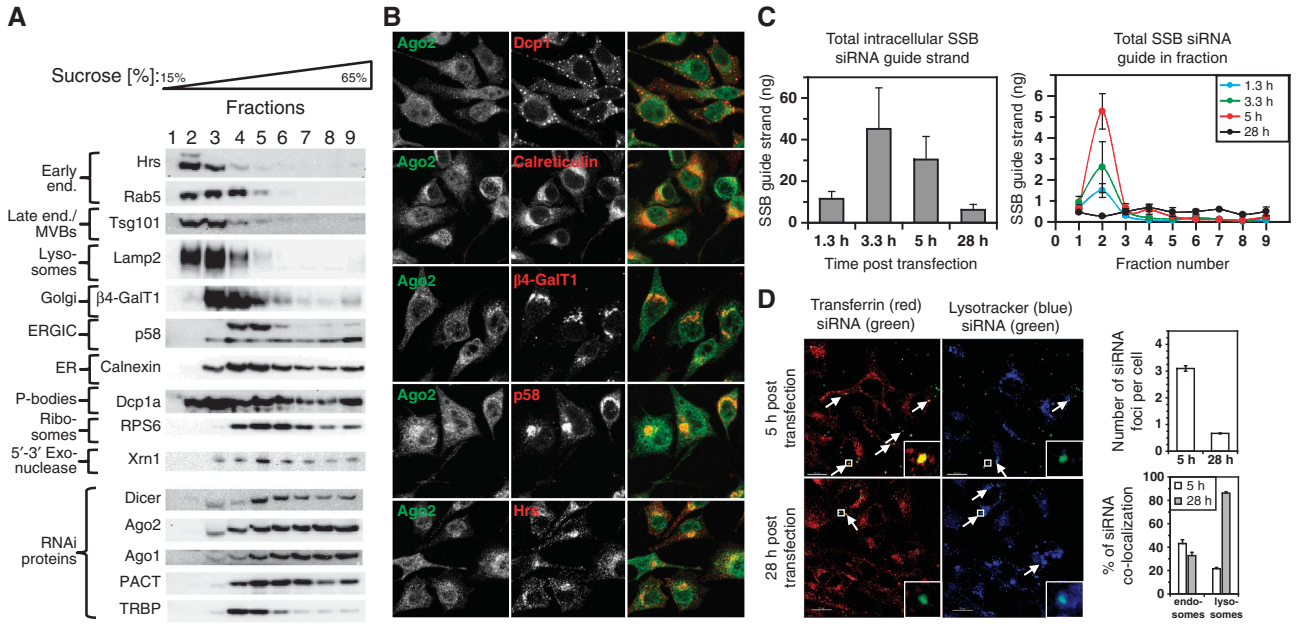

Figure 1 Ago2 and siRNAs localize to a number of different compartments. (**A**) Western blot analysis of sucrose gradient fractions. (**B**) Immune fluorescence of HeLa cells stained with anti-Ago2 and counterstained with antibodies against marker proteins for P-bodies (Dcp1), ER (Calreticulin), Golgi (β4-GalT1), ERGIC (p58) and early Endosomes (Hrs). Settings were chosen so that no background was detected from cells stained only with secondary antibodies, all images were taken with the same settings. (**C**) RT–qPCR quantification of total intracellular SSB guide strand (left panel) and in the sucrose fractions (right panel) at the indicated time points post transfection. (**D**) Life cell imaging of HeLa cells transfected with 5′TMR-labelled HuR siRNAs (green) and counterstained with Lysotracker (lysosome marker; blue) or transferrin (endosome marker; red). Source data for this figure is available on the online supplementary information page.

dependent manner (Jakymiw *et al*, 2005; Jagannath and Wood, 2009). Other reports have demonstrated a link between RNAi and membranes (Cikaluk *et al*, 1999; Tahbaz *et al*, 2001, 2004; Gibbings *et al*, 2009; Lee *et al*, 2009; Gibbings and Voinnet, 2010). In early reports, Dicer and Ago2 have been shown to fractionate with membranes (Tahbaz *et al*, 2004) and to co-localize with the Golgi apparatus (Cikaluk *et al*, 1999; Tahbaz *et al*, 2001; Barbato *et al*, 2007). Furthermore, disruption of the Hermansky Pudlak 1 and 4 proteins (HPS1, HPS4), which are implicated in membrane trafficking and function (Huizing *et al*, 2000), accelerate the loading of Ago2 with siRNAs in flies (Lee *et al*, 2009). Additionally, it has been proposed that RISC assembly and disassembly is linked to membranes of the endo-lysosomal system (Gibbings *et al*, 2009; Lee *et al*, 2009; Gibbings and Voinnet, 2010). Given that there is still no clear picture about the sites of RISC loading, target mRNA association and silencing, in this work we aimed to quantitatively and spatially follow the siRNA fate within the cell upon lipid delivery from initial uptake and subcellular redistribution to its entry into the RNAi pathway, and to identify the sites of RNAi activity.

Results

Ago2, siRNAs and miRNAs localize to a number of different compartments

To characterize the intracellular distribution of RNAi pathway proteins, exogenously added siRNAs, and endogenous miRNAs, HeLa cells were transfected by lipofection with siRNAs against SSB (Pei *et al*, 2010) (Sjogren syndrome antigen B), lysed after 24 h and the post-nuclear detergent-free supernatants were fractionated on continuous density sucrose gradients (Figure 1A). Markers for lysosomes (Lamp2), endosomes and multi-vesicular bodies (MVBs; Hrs, Rab5, Tsg101) were enriched in fractions 2 and 3 (20–33% sucrose), markers for Golgi (β4-GalT1) in fractions 3–5, the ER-Golgi intermediate compartment (ERGIC; p58), the ER (Calnexin) and ribosomes (RPS6) in fractions 4–7 (42–64% sucrose), confirming the expected fractionation pattern consistent with fractionation of cytoplasmic lysates in previous studies (e.g., Gibbings *et al*, 2009; Jouannet *et al*, 2012). Ago2 showed a broad distribution and was present throughout fractions 3–9. Similarly, Ago1, Dicer and PACT fractionated broadly, whereas only TRBP showed evidence for a more confined localization and co-sedimented sharply with Golgi and ER marker proteins (Figure 1A). The fractionation of the RNAi pathway proteins did not change upon the transfection of an siRNA, suggesting that a transfected siRNA does not induce a major redistribution of these proteins (Supplementary Figure S1A).

To confirm the general fractionation pattern of endogenous Ago2, we performed immune fluorescence (IF) of Ago2 as well as the different organelle marker proteins in HeLa cells (Figure 1B). The established high specificity of the Ago2 antibody (clone 11A9) (Rüdel *et al*, 2008) was validated also in our hands using a peptide comprising the antigenic epitope (Supplementary Figure S1B). Ago2 staining showed the typical diffuse punctuate pattern throughout the cytoplasm with the typical enrichment in the perinuclear region and a half-moon shaped structure (Golgi) and some individual strong foci (P-bodies). In accordance with the broad fractionation of Ago2, endogenous Ago2 also co-localized by IF partially with the ER, ERGIC, Golgi, P-bodies and early

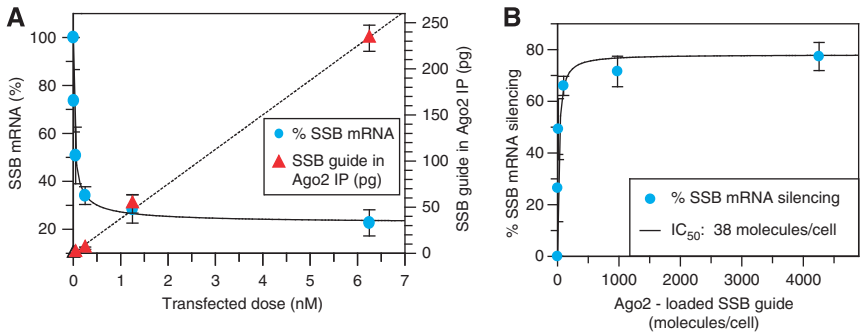

Figure 2 Excess of inactive siRNA masks active population. (**A**, **B**) Ago2 IPs were performed in a quantitative manner 24 h after the HeLa cells were transfected with SSB siRNA. mRNA levels were determined by RT–qPCR from purified total RNA.

endosomes (Figure 1B). This intracellular distribution of endogenous Ago2 is consistent with previous publications, where Ago2 was shown to partially co-localize with Golgi (Cikaluk *et al*, 1999; Tahbaz *et al*, 2001), P-bodies (Liu *et al*, 2005; Pillai *et al*, 2005; Sen and Blau, 2005; Leung *et al*, 2006; Ohrt *et al*, 2008; Zeng *et al*, 2008; Jagannath and Wood, 2009; Pare *et al*, 2009) or endosomes (Gibbings *et al*, 2009; Lee *et al*, 2009). Additionally, our data confirm the general notion that endogenous Ago2 appears to distribute differently than Ago2-GFP, which was shown to strongly accumulate in P-bodies (Liu *et al*, 2005; Sen and Blau, 2005; Leung *et al*, 2006; Ohrt *et al*, 2008; Jagannath and Wood, 2009). Consistent with an accumulation in P-bodies, we found overexpressed Ago2-GFP enriched in the Dcp1 containing fractions (4–6) of the continuous sucrose density gradient (Supplementary Figure S1C).

As the overall Ago2 localization was not instructive about sites of RNA silencing activity, we next followed the siRNA during onset of uptake and a potential subsequent subcellular redistribution to monitor its putative entry into the RNAi pathway. HeLa cells were transfected with the SSB siRNA and a control siRNA with no target in human cells (pGL3), harvested after 1.3, 3.3, 5 and 28 h and fractionated as above. During the 5-h transfection period, the SSB siRNA was increasingly enriched in the endo-/lysosomal fractions. After 28 h, the cells were cleared of 75–90% of the transfected siRNAs by secretion and/or degradation (Figure 1C; Supplementary Figure S1D), whereas the remaining siRNA was now mostly in the non-endosomal fractions, suggesting that only 10–25% of the transfected siRNA ever had the potential to load into RISC. In accordance with a strong accumulation and degradation of the siRNA in endosomes and lysosomes, respectively, a transfected TMR-labelled siRNA co-localized with endosomal (transferrin) and lysosomal (LysoTracker) markers in living cells and co-sedimented with these organelles in sucrose gradients (Figure 1D; Supplementary Figure S1E–G), suggesting that the bulk of transfected siRNA enters the cells through the endosomal system (Lu *et al*, 2009), and that the major fraction of the transfected siRNA is quickly targeted to lysosomes for degradation. Interestingly, the non-targeting pGL3 siRNA fractionated similar to the SSB siRNA, suggesting that bulk trafficking of siRNAs is not driven by the presence of a target mRNA (Supplementary Figure S1D). Given this dramatic clearance of siRNA within the initial phase of transfection, we reasoned that at late time points, the remaining amount of siRNA might better reflect the active population. Indeed, siRNA remaining at 28 h fractionated in a sucrose gradient similarly as endogenous miR-16 (Supplementary Figure S1H), a representative and relatively abundant miRNA in HeLa cells, indicating that, once in the cytoplasm, siRNA is subject to similar protein interactions and trafficking events as endogenous miRNAs. However, both, miR-16 and the SSB siRNA were present in all Ago2 containing fractions, suggesting that even after initial clearance, the co-fractionation of RNAi factors and siRNAs or miRNAs is also not indicative to discern the active siRNA/Ago2 population.

Excess of inactive siRNA masks active population

Using Ago2 immune precipitations (IPs), we next quantified how much of the siRNA residing in the cell after the initial major clearance wave is loaded into Ago2. Ago2 IPs (Rüdel *et al*, 2008) were quantitatively highly reproducible (Supplementary Figure S2A and B), and importantly, showed a linear correlation between eluted Ago2 and the amount of input lysate over the relevant range of sample concentration (Supplementary Figure S2C). Also, the IP efficiency of Ago2 was independent of the sucrose concentration as confirmed for both, the continuous (Supplementary Figure S2D) and discontinuous sucrose gradients (Supplementary Figure S2E) used in this study. Additionally, to rule out that loaded siRNA might get lost during the IP procedure due to dissociation from Ago2 and to unambiguously confirm that the IP procedure allows to quantitatively determine the amount of complex, we used 5'TMR-labelled single-stranded HuR siRNA complexed to recombinant Ago2 *in vitro* as a standard to quantify siRNA recovery by RT–qPCR, which yielded a relative recovery of Ago2–siRNA complexes in the protein IP of 83% (Supplementary Figure S2F). In addition, fluorescence anisotropy measurements confirmed that the recovered siRNA was still mostly complexed with Ago2 after native elution with the antigenic peptide (Supplementary Figure S2G). This data demonstrates the stability of the complex throughout the IP procedure, consistent with the long half-life of Ago2-guide strand complexes *in vitro* (half-life of Ago2-guide strand >20 h; Supplementary Figure S2H) and the high stability of the complex reported previously (Martinez and Tuschl, 2004), and altogether unambiguously confirm that the IP procedure allows to quantitatively determine Ago2-loaded siRNA within a range of $\pm 20\%$ accuracy.

HeLa cells transfected with increasing doses of the very potent SSB siRNA reached saturation of the mRNA knockdown already at 0.25 nM transfected siRNAs, with an IC_{50} of 24 ± 4 pM (Figure 2A). In contrast, the amount of loaded

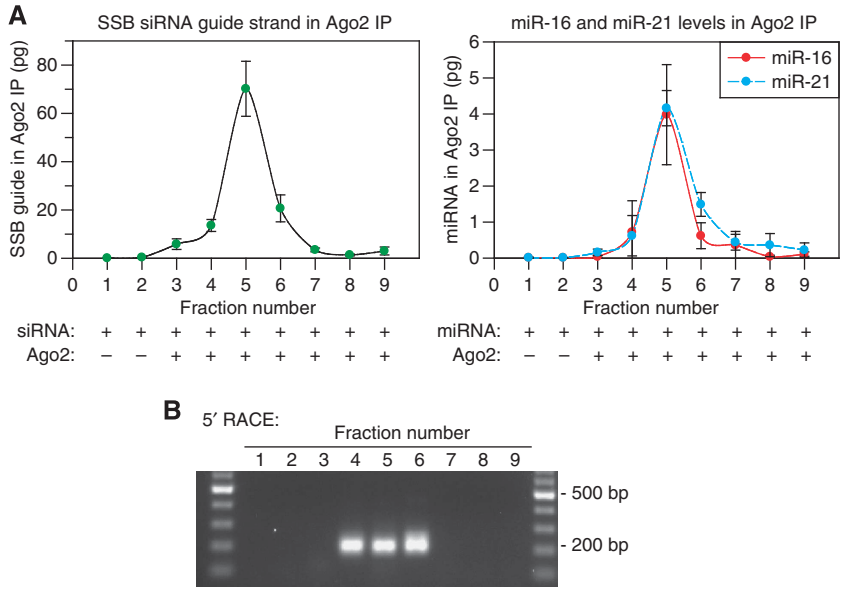

Figure 3 siRNA- and miRNA-loaded Ago2 complexes and mRNA slicing product co-sediment with ER/Golgi membranes. (**A**) Ago2 IPs were performed from fractions of the sucrose gradient displayed in Figure 1A, and SSB siRNA guide strand, miR-16 and miR-21 were quantified by RT–qPCR. (**B**) 5′RACE performed with total RNA from each of the sucrose gradient fractions of the gradient displayed in Figure 1A. PCR products were separated on an agarose gel, a positive 5′RACE signal results in a 208-bp fragment. Source data for this figure is available on the online supplementary information page.

guide strand in Ago2 increased almost linearly up to the highest transfected dose (6.25 nM; Figure 2A, Supplementary Figure S2K and L). Consistent with observations emerging from previous *in vivo* studies (Pei *et al*, 2010), our data suggest that at siRNA concentrations beyond saturation of knockdown, a depot of loaded Ago2 may be formed and that the capacity of the RISC loading machinery is not yet saturated, at least for SSB siRNA concentrations of up to 200- to 300-fold beyond the IC_{50} (Figure 2A). Further calculations reveal that the IC_{50} of SSB mRNA knockdown is as little as 35–40 molecules of siRISC per cell (Figure 2B). To investigate whether these low numbers of siRISC per cell required for a 50% mRNA knockdown is a general feature of siRNAs, we performed the analogous experiments with absolute quantification for three additional siRNAs of markedly different potency (Supplementary Figure S2N–P). Two siRNAs were targeting other mRNAs (GAPDH and HuR), the third siRNA ('SSB(53)') targets another site within the same mRNA (SSB) but with significantly lower overall potency. Strikingly, for all of these siRNAs we find equally low numbers at IC_{50} ranging from 10 to 110 siRISC molecules per cell. These data suggest that RNA silencing is in general a remarkably efficient process once the siRNA is loaded into RISC. Additionally, we quantified the fraction of Ago2-loaded siRNA in relation to total intracellular siRNA which followed a hyperbolic saturation curve with increasing siRNA dose, with $<1\%$ fraction bound at the IC_{50} of knockdown and saturating at ca 4% maximal loading (Supplementary Figure S2I, J and M). This behaviour suggests that either compartmentalization or other limiting factors prevent a quantitative loading of the intracellular siRNA material into Ago2. Considering estimate accuracies of our correction for the efficiencies of all experimental steps characterized in detail above, this data suggest that even at maximum experimental underestimation, a major fraction of intracellular siRNA but also miRNA (see Figure 4B and Supplementary Figures S1H and S3B) is non-RISC associated, which may appear counter intuitive to the current assumption in the field. Interestingly however, a recent publication (Janas *et al*, 2012) reports a conclusion perfectly consistent with our quantitative data. Based on an absolute quantification of Ago proteins and total miRNA copies per cell, the authors come to the conclusion that there is a 13-fold excess of miRNA over Argonaute molecules in HeLa cells. This implies that only a few per cent of a given miRNA will be loaded in Ago proteins on average, in line with the data we show in Figure 4B and Supplementary Figures S1H and S3B.

Active siRISC co-sediments with ER and Golgi membranes

Given that such a minor fraction of intracellular siRNA gets loaded into Ago2, we concluded that for localization of siRNA activity, tracing bulk siRNA with microscopy or fractionation becomes very misleading. Therefore, we further refined the cell fractionation analysis of the siRNA by performing Ago2-IPs from continuous density sucrose gradients to quantify the amount of siRNA and miRNA loaded in Ago2 in each fraction. IP efficiencies were comparable across the gradient and well reproducible between independent fractionation experiments (Supplementary Figure S2D and E). Surprisingly and in contrast to the broad bulk distribution of siRNA, miRNA and RNAi pathway proteins, the Ago2-loaded SSB siRNA, miR-16 and miR-21 all eluted in a sharp peak in the Golgi and ER fractions (fractions 4–6; Figure 3A), suggesting that the active siRNA/miRNA population may be associated with Golgi and/or ER membranes. To get further evidence for activity of the siRNA-Ago2 complexes (siRISC) in these fractions, we next performed 5′RACE with RNA purified from each fraction to qualitatively assess the absence or presence of the cleavage product of the SSB mRNA. Consistent with the fractionation of the siRISC, a 5′RACE product was only detected in fractions 4–6 (Figure 3B). Sequencing of the 200 bp 5′RACE PCR product confirmed that all sequenced clones contained SSB

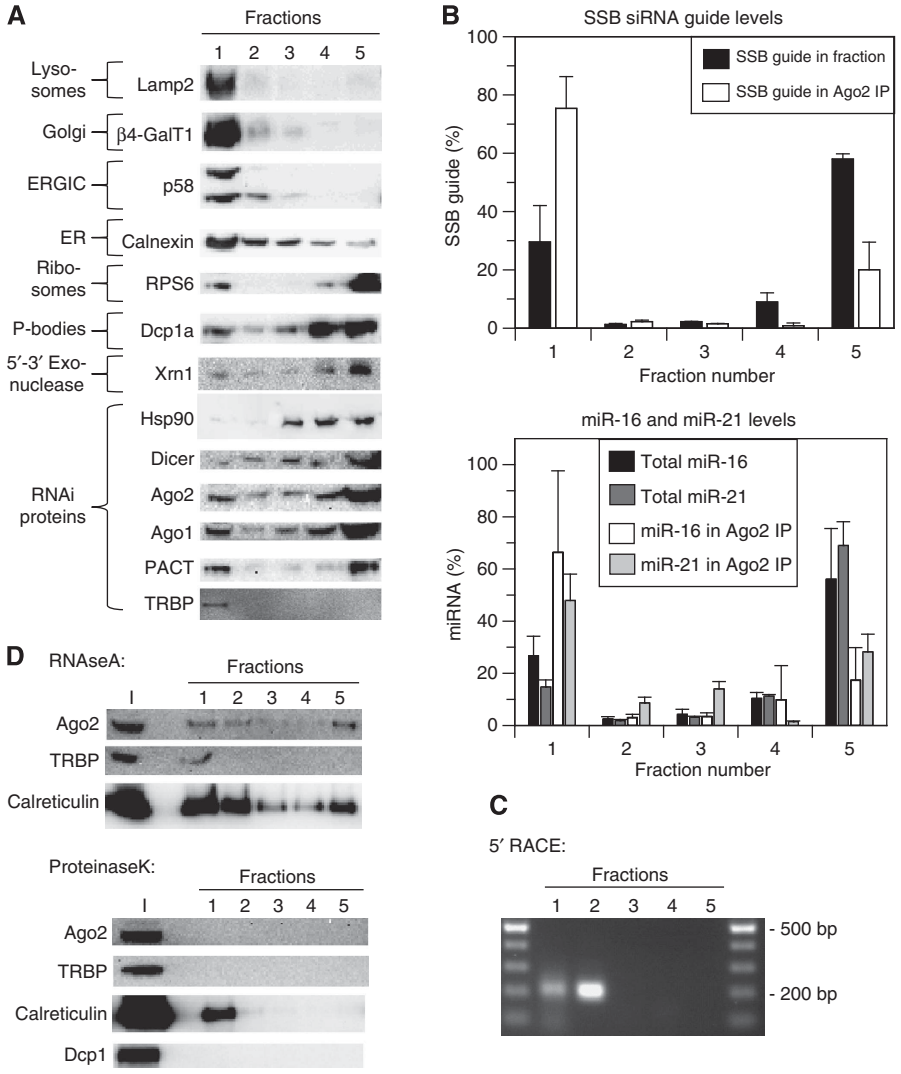

Figure 4 Active siRISC associates to the outside of membranes. HeLa cells were transfected with SSB siRNA and subjected to a membrane floatation assay. Fractions were analysed by western blotting (**A**), Ago2 IP and RT–qPCR (**B**) and 5′RACE (**C**) as in Figure 3. (**D**) HeLa lysates were treated with RNAseA or ProteinaseK and subjected to membrane floatation assays, fractions were analysed by western blotting. RNAse A activity was confirmed by analysis of GAPDH mRNA levels in the sucrose gradient fractions after the treatment (Supplementary Figure S3C). Source data for this figure is available on the online supplementary information page.

mRNA cleaved at the expected position (Supplementary Figure S3A). Additionally, we tested the distribution of the cytoplasmatic 5′ to 3′ exonuclease *Xrn*1 in the same sucrose gradient fractions (Figure 1A). *Xrn*1 was present in all non-endo/lysosomal fractions and enriched in fractions 4–6. This shows that the sliced mRNA can even be detected in fractions where it can be degraded and in turn excludes the possibility that the absence of 5′RACE products in the fractions 1–3 and 7–9 was due to immediate mRNA degradation after the siRNA-mediated mRNA slicing. In summary, these experiments show that siRISC as well as the sliced mRNA do co-fractionate with Golgi and ER membranes.

Active siRISC associates to the outside of the rER

To investigate whether the active siRISC also physically associates with membranes, post-nuclear lysates of HeLa cells transfected with SSB siRNA were subjected to a membrane floatation assay on a discontinuous sucrose gradient (Tahbaz *et al*, 2004). After the centrifugation, membrane proteins of Lysosomes, Golgi and ER were enriched on the top (fraction 1 and partially 2), whereas non-membrane bound material remained in the loading zone (fractions 3–5; Figure 4A). Consistent with a previous report (Tahbaz *et al*, 2004), a portion of the cytoplasmatic population of Ago2 and Dicer, but also a fraction of Ago1 and PACT floated with membranes; Interestingly, TRBP was exclusively membrane associated. While the major siRNA, miRNA as well as Ago2 amounts were found in the non-membrane fractions, loaded siRISC as well as miRISC (miR-16 and miR-21) were strongly enriched in the membrane fractions (Figure 4B; Supplementary Figure S3B). Additionally, the SSB mRNA cleavage product floated exclusively with membranes (Figure 4C), whereas again, *Xrn*1 was present in all fractions (Figure 4A). Together, this suggested that the siRISC activity is not only co-fractionating with Golgi and ER membranes but is indeed membrane associated. To further characterize the Ago2 association with membranes, HeLa lysates were treated with RNAseA or ProteinaseK, and subsequently subjected to membrane floatation assays. RNAseA treatment did not lead to a detectable reduction in Ago2 in the membrane fraction

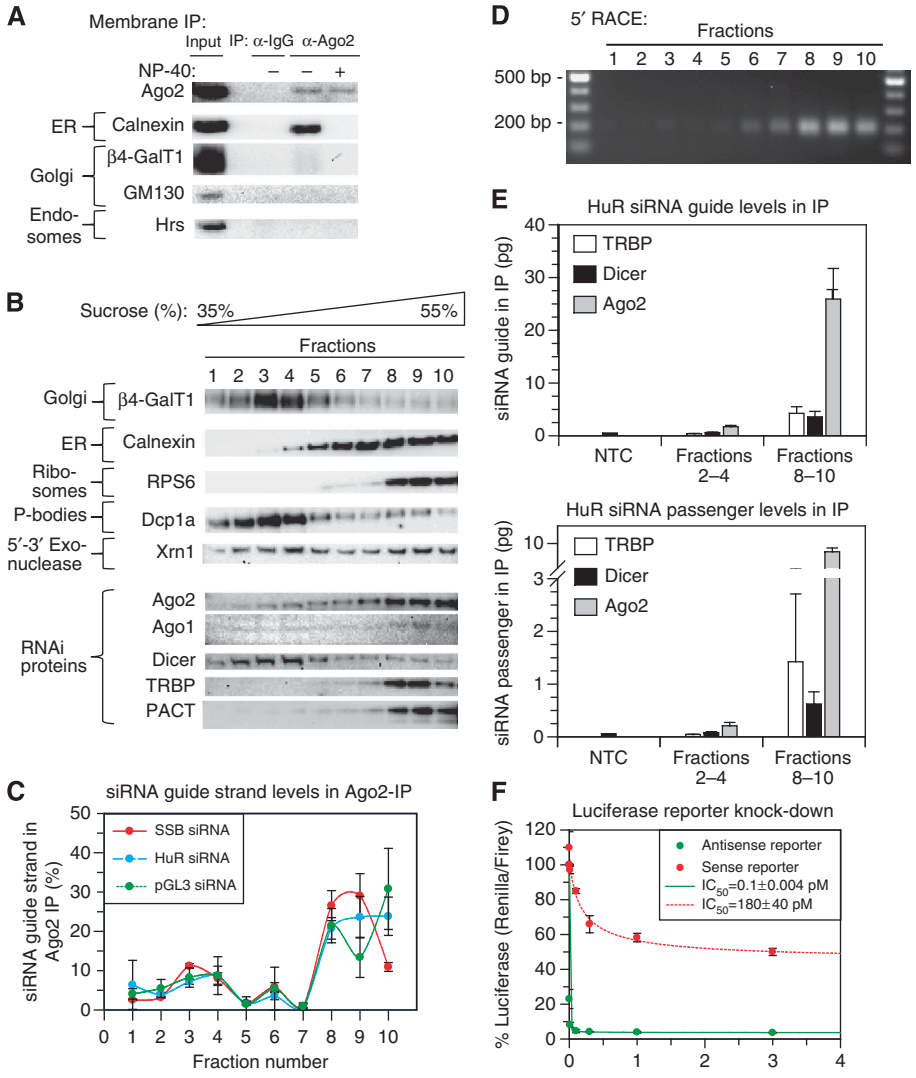

Figure 5 siRISC loading and siRNA-mediated mRNA cleavage occur on the membrane of the rough endoplasmatic reticulum. (**A**) Membrane IPs were performed with HeLa lysates (as described in Materials and methods) and eluates were analysed by western blotting. (**B**) HeLa cells were transfected with SSB, HuR and pGL3 siRNA and subjected to a sucrose sedimentation gradient. Fractions were analysed by western blotting, Ago2 IP and RT–qPCR (**C**) and 5′RACE (**D**). (**E**) HeLa cells transfected with HuR siRNA were subjected to a sucrose sedimentation gradient as in (**A**). The Golgi/P-body fractions (2–4) and rER fractions (8–10) were pooled and used for TRBP, Dicer and Ago2 IPs. The eluates were analysed by RT–qPCR. Averages of one typical experiment are shown, error bars represent standard deviation of the RT–qPCR. (**F**) A dual-luciferase reporter plasmid was co-transfected together with increasing concentrations of the HuR siRNA, luciferase activity was measured after 24 h. Source data for this figure is available on the online supplementary information page.

(Figure 4D and Supplementary Figure S3C, corresponding non RNAse treated reference data in Figure 4A), indicating that indirect association via the target mRNA does not play a major role for Ago2 membrane association. Additionally, given that Ago2 membrane association is independent of RNA (Figure 4D), this rules out that Ago2 membrane association is mediated through polysomes.

Upon ProteinaseK treatment, all Ago2 was lost from the membrane fraction (Figure 4D). As controls, also Dcp1a which is not supposed to be encapsulated by membranes was fully susceptible to ProteinaseK treatment, whereas Calreticulin as an ER luminal protein was entirely protected from degradation and only detectable in the membrane fraction. In consequence and consistent with a previous report (Cikaluk *et al*, 1999), this data demonstrates that Ago2 associates to the cytosolic rather than the luminal side of membrane enclosed compartments.

Finally, to unambiguously corroborate the physical association of Ago2 and RISC with membranes by an additional orthogonal method and to identify the membranes Ago2 associates with, HeLa cells were treated with Nocodazole and CytochalasinD to disrupt the cytoskeleton, lysed in the absence of detergents, and an IP against Ago2 was performed to pull down the Ago2-associated membranes. Species that were indirectly immune precipitated via membranes were subsequently recovered by mild elution with an NP-40 containing buffer. IP with the anti-Ago2 antibody brought down the ER membrane marker Calnexin, but no markers of Golgi or endosomal membranes, demonstrating a specific physical association of Ago2 with the membrane of the ER (Figure 5A). As negative control, the anti-Ago2 IP was performed already in the presence of NP-40, thereby omitting any lipid mediated interactions. Under these conditions, no Calnexin was detectable in the eluate, which confirms that

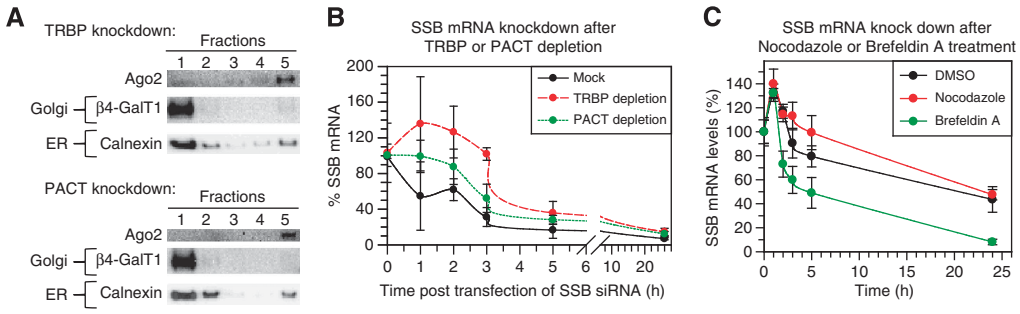

Figure 6 Membrane anchoring of RISC by TRBP/PACT accelerates RNA silencing. (**A**) HeLa cells depleted of TRBP or PACT were subjected to membrane floatation assays as in Figure 4A, fractions were analysed by western blotting. (**B**) HeLa cells depleted of TRBP and/or PACT were transfected with SSB siRNA and harvested after the indicated time points. Relative SSB mRNA levels, normalized to GAPDH mRNA, were quantified by RT–qPCR. (**C**) HeLa cells were pre-treated with Nocodazole (5 μg/ml) or Brefeldin A (10 μg/ml) for 2 h, transfected with the SSB siRNA at 0.5 nM, and lysed at the indicated time points after the transfection. SSB mRNA levels were analysed by RT–qPCR. Source data for this figure is available on the online supplementary information page.

the interaction of Ago2 with Calnexin is membrane mediated. As an additional control, in a similar IP with mouse IgG, none of the membrane marker proteins was detectable (Figure 5A). To confirm that, as indicated by the fractionation (Figure 4A), not only Ago2 but also the RISC and RLC factors associate with the ER, HeLa cells were subjected to sedimentation gradients optimized for purification of ER membranes (Figure 5B) followed by membrane immune precipitations. First, the fractions containing the membranes of the rER (fractions 8–10) were pooled and used for a membrane IP specific for the ER membrane protein calnexin (Supplementary Figure S4A). Strikingly, Ago2, TRBP and Dicer were all present in the eluate from the anti-calnexin membrane IP, indicating that the factors constituting RLC and RISC associate with the rough endoplasmic reticulum (rER) membrane. Consistent with these data it has been shown previously by IF that *x. laevis* TRBP co-localizes with the ER (Eckmann and Jantsch, 1997), and that TRBP and Dicer co-localize predominantly in the perinuclear region in HeLa cells (Daniels *et al*, 2009). As an additional control, anti-Golgi membrane IPs were performed with the fractions containing Golgi membranes (fractions 2-4). Neither Ago2, nor Dicer, nor TRBP were enriched in the Golgi IP eluate compared to the IgG negative control IP (Supplementary Figure S4A). Altogether, these data provide strong evidence that RLC and siRISC are bound to the cytosolic surface of the rER membrane.

siRNA-mediated target mRNA cleavage occurs on the rER

After having found that siRNA-loaded Ago2 floats with membranes, that Ago2 associates specifically with the ER membrane, and that siRNA-loaded Ago2 as well as the slicing product co-fractionate with ER as well as Golgi markers, we wanted to further refine at which of these compartments siRNA mediated target cleavage occurs. HeLa cells transfected with SSB, HuR and pGL3 siRNAs were subjected to sedimentation gradients optimized for purification of ER membranes. In these gradients, Golgi membranes were enriched in fractions 2–4, membranes of the smooth ER in fractions 5–7 and membranes of the rER, revealed by the additional presence of the ribosomal protein RPS6, in fractions 8–10 (Figure 5B). In agreement with the fractionation data in Figure 1A, also after separation of Golgi from ER factions, Ago2 and Dicer indeed co-sedimented with both membranes (Cikaluk *et al*, 1999; Tahbaz *et al*, 2001). Interestingly, Ago1 and Ago2 were most abundant in the fractions of the rER, whereas Dicer peaked in the Golgi-/P-body fractions. Consistently, Dicer had previously been observed to co-localize with Golgi and ER in rat primary neurons (Barbato *et al*, 2007). TRBP and PACT again showed a very confined localization and co-sedimented exclusively with the rER, in consistence with early work in *X. laevis* reporting cytoplasmic TRBP to localize to the ER and/or polysomes (Eckmann and Jantsch, 1997). Again, the bulk siRNA fractionated broadly throughout the gradient (Supplementary Figure S4B). After IP of Ago2 from the fractions however, we observed two distinct pools of siRNA-loaded Ago2, the major population co-sedimenting with the rER (Figure 5C). A second, minor pool of siRISC was detected in fractions containing not only Golgi membranes but also the P-body marker Dcp1, which, in these gradients peaks together with the Golgi markers. In fact, in light of the absence of significant Golgi association as determined by Ago2 membrane IPs (Figure 5A), it appears more plausible that this second minor population of siRISC is P-body rather than Golgi associated. Interestingly, the non-targeting pGL3 siRNA loaded into Ago2 also co-sedimented predominantly with rER identical to the targeting siRNAs (Figure 5C, HuR and SSB siRNAs), further supporting that this fractionation is independent of a target mRNA and not dependent on polysomes. We next wanted to address whether these two spatially separated siRISC pools represent functionally different complexes, or rather complexes of different maturation state. As, *ex vivo*, both pools of immune purified Ago2 were competent of *in vitro* mRNA slicing we concluded that both complexes comprise mature siRISC (Yoda *et al*, 2010), that is, slicing competent RISC with single-stranded guide siRNA (Supplementary Figure S4C). As this does not necessarily imply that alike *ex vivo*, slicing indeed occurs in both compartments within the cell, we again performed 5′RACE on all fractions to detect the endogenous slicing product. Strikingly, the endogenous mRNA cleavage product co-sedimented exclusively with membranes of the rER (Figure 5D), strongly suggesting that the site of endogenous mRNA silencing, at least for siRNA, is the rER.

Canonical RISC loading occurs at the rER

We next aimed to address whether the rER is also the site of RISC loading, or whether instead the additional, minor Golgi/

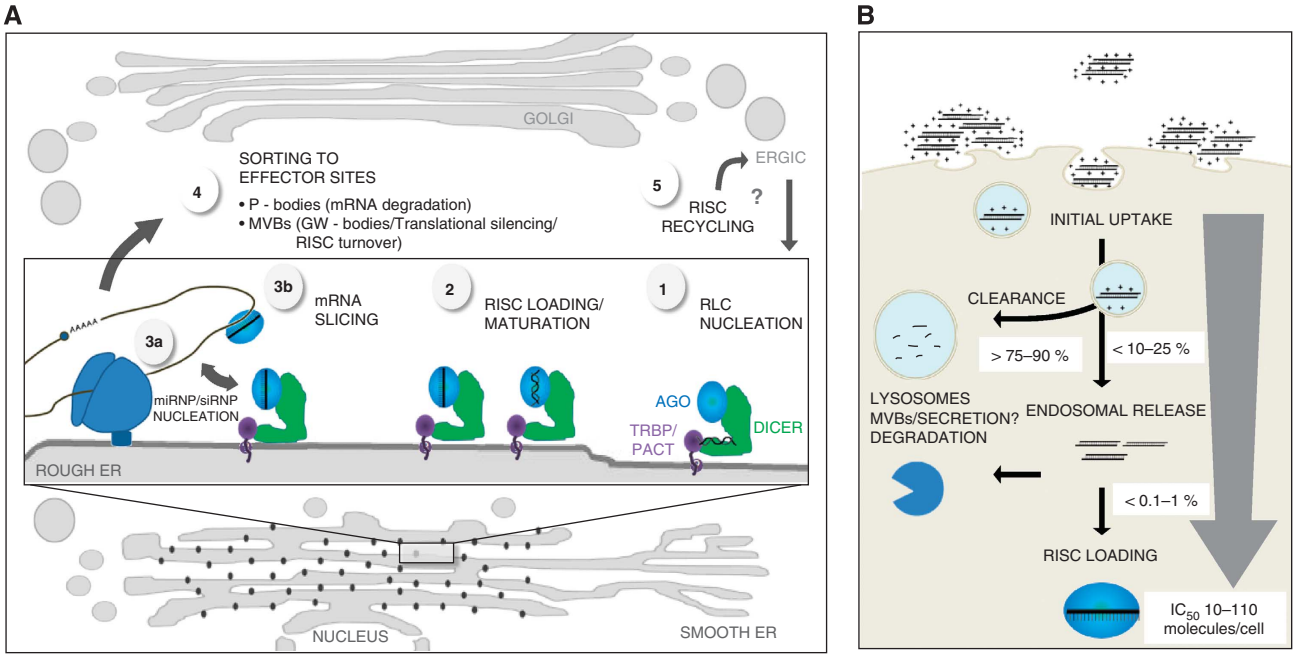

Figure 7 Model for spatial organization of the RNAi pathway and quantitative fate of siRNA following transfection. (**A**) Based on the data presented in this work, we propose that the central steps of RNAi occur at the cytosolic surface of the rER membrane. Exposure of ds siRNA to RLC, anchored to the membrane either directly or indirectly via TRBP and/or PACT, is nucleated by encounter of all partners at the rER (1). Upon transfer of the ds siRNA from RLC into Ago and passenger strand removal (RISC loading and maturation, (2) mature RISC is formed. rER association provides mature RISC a privileged position to sample over translationally active mRNAs which either permanently (secreted/membrane proteins) or transiently (soluble proteins) associate with the rER (Lerner *et al*, 2003; Gerst, 2008; Chen *et al*, 2011). Upon encounter of a target mRNA, the formation of an siRNP or miRNP is nucleated (3a) and a perfect target gets endonucleolytically sliced by Ago2 (3b). Considering previous reports, it is likely that the RISC-associated RNPs are then further directed to effector sites for downstream silencing events (4), such as P-bodies for exposure to the mRNA degradation machinery (Eulalio *et al*, 2007a), or MVBs/GW bodies for interaction with GW proteins and/or RISC disassembly (Gibbings and Voinnet, 2010). Finally, 'consumed' RISC may get either eliminated, or reactivated and recycled back to the ER through the highly dynamic endomembrane apparatus or other routes (5). (**B**) In summary of the data presented in Figure 1 and Supplementary Figure S2, following endosomal uptake of siRNA with cationic lipofection a lion's share of the intracellular siRNA is cleared again very quickly via lysosomes and potential additional secretion or degradation pathways. Even though the RISC loading machinery is not saturated (Figure 2A), the residual intracellular siRNA is loaded very inefficiently into Ago (<0.1–1% of the initial intracellular siRNA). This explains why, although as little as 10–110 loaded RISC molecules per cell are sufficient to promote knockdown of a relatively abundant mRNA such as SSB, the cell needs to be flooded with siRNA by exposure to nanomolar concentrations to sustain significant mRNA knockdown.

P-body population of siRNA-Ago2 might account for complexes engaged in loading. The canonical RLC was proposed to comprise Ago2, Dicer and TRBP (Gregory *et al*, 2005; Maniataki and Mourelatos, 2005; Chendrimada *et al*, 2007; MacRae *et al*, 2008; Noland *et al*, 2011). We have shown that all three proteins float with membranes (Figure 4A), and can be pulled down in a membrane IP with an ER membrane protein (Supplementary Figure S4A). Furthermore, TRBP does exclusively co-fractionate with the rER, and also Ago2 and Dicer partially co-fractionate with the rER (Figure 5B). This supports that a canonical RLC may form on the rER rather than at Golgi or P-bodies where TRBP and PACT are absent. To further corroborate this hypothesis, lysates of siRNA-transfected HeLa cells were subjected to a Golgi/ER gradient as in Figure 5B. For qPCR detection sensitivity reasons of the passenger strand, we focused on the HuR siRNA rather than the SSB siRNA in these experiments. After pooling each, the Golgi/P-body fractions (2–4) as well as the rER fractions (8–10), IPs for TRBP, Dicer and Ago2 were performed (Figure 5E). In the TRBP and Dicer IPs, both guide and passenger strand of the HuR siRNA were detectable in the rER fractions, suggesting that TRBP and Dicer are associated with double-stranded siRNA in these fractions. Consistent with the Ago2 IPs from the other gradients, Ago2 bound HuR siRNA guide strand was again detectable in both the Golgi/P-body and in the rER fractions; however, the Ago2-associated passenger strand was clearly enriched in the rER fraction. Moreover, despite the dramatically higher amounts of Dicer in the Golgi/P-body fractions, neither guide nor passenger strand was detectable in this pool but clearly enriched in Dicer immune precipitates from the rER fractions. Together, these data strongly suggest that the rER fractions comprise both mature siRISC and full RLC associated with double-stranded siRNA (and potentially single-stranded siRNA as well), whereas the Golgi/P-body pool of loaded Ago2 consists of >98% mature siRISC with guide strand only, as well as non-siRNA-associated Dicer.

To further corroborate this conclusion, we wanted to rule out the possibility that the detected HuR sense strand in the eluates resulted from sense strand misloaded as guide rather than siRNA duplex. While bioinformatic analysis supported a high asymmetry and therefore antisense strand selectivity for the HuR siRNA (Supplementary Figure S4E), we additionally designed a Firefly/Renilla dual luciferase reporter containing either the target site of the antisense or the sense strand in the 3′ UTR, and co-transfected these plasmids together with the HuR siRNA into HeLa cells. With an IC_{50} of 0.2 nM the passenger strand was >1000-fold less active than the guide

strand which had an IC_{50} of 0.1 pM (Figure 5F; Supplementary Figure S4D), confirming that strand selection for this siRNA is highly biased to the antisense strand and that loading of sense strand as guide can be neglected. Therefore, we conclude that Ago2 in the rER fractions is indeed partially associated with double-stranded siRNA and comprises not only mature siRISC but also complexes engaged in loading, that is, a 'pre-RISC state' (Kawamata and Tomari, 2010; Czech and Hannon, 2011). Altogether, this data suggests that also canonical RISC loading of Ago2 through Dicer and TRBP/PACT occurs at the membranes of the rER.

Membrane anchoring of RISC is dependent on TRBP and PACT

Given that TRBP and PACT did co-sediment with strong enrichment at the ER membrane, we speculated that Ago2 might be anchored to the membranes (potentially indirectly) via either of these proteins. We thus depleted TRBP or PACT by RNAi (Supplementary Figure S5A), and subjected the post nuclear lysates to membrane floatation assays. The Ago2 protein levels were similar in control cells and in the cells with TRBP or PACT knockdown (Supplementary Figure S5A), but in contrast to the mock or RNAseA-treated lysates (Figure 4D), the amount of membrane-associated Ago2 was strongly reduced after TRBP depletion and completely abolished after PACT depletion (Figure 6A). Additionally, in a membrane IP with antibodies against Ago2, the amount of co-eluted marker proteins for the ER and ribosomes was reduced when TRBP or PACT was depleted as compared to mock-treated cells (Supplementary Figure S5B and S5C). Interestingly, the smaller effect of TRBP knockdown on Calnexin association with Ago2 as compared to the more dramatic effect upon PACT knockdown mirror images the efficiency of the knockdown of the two proteins. This data suggests that Ago2 associates with membranes through TBRP and PACT, most plausibly indirectly through the complex of TRBP and PACT with Dicer.

Nucleation of RISC loading and mRNA slicing at the rER membrane is important for kinetic and thermodynamic efficiency of RNAi

Results from previous publications about whether TRBP and PACT are required for siRNA-mediated RNA silencing are contradictory (Haase *et al*, 2005; Kok *et al*, 2007). Given that as little as 10–110 molecules of siRISC per cell are sufficient for 50% knockdown of three different, relatively abundant mRNAs (Figure 2B; Supplementary Figure S2N–P), but that the onset of RNAi after transfection is extremely fast, we reasoned that the sequestration of active Ago2 to membranes may be responsible for accelerating the silencing kinetics. This would imply that TRBP and/or PACT as membrane anchors may not be qualitatively required for RNAi but might rather play a main role in the quantitative efficiency and particularly the kinetics of the onset of silencing. To test this hypothesis, we transfected the SSB siRNA into TRBP/PACT RNAi-depleted versus mock-treated cells. Consistent with our hypothesis, the onset of SSB mRNA knockdown was clearly delayed when TRBP or PACT had been depleted (Figure 6B). After 24 h, also in TRBP/PACT-depleted cells knockdown had caught up to reach saturation, most likely explaining why TRBP and PACT had not been found to be essential for RNAi in earlier reports. In addition, we tested whether perturbation of directional cytoskeleton-dependent cell transport to the ER would result in a similar delay in the onset of silencing. HeLa cells were pre-treated for 2 h with Nocodazole (5 μg/ml) prior to transfection with the SSB siRNA, and the knockdown was quantified at various time points after transfection by RT–qPCR (Figure 6C). Indeed, the onset of silencing was delayed. While this is again consistent with subcellular localization being important for the kinetic efficiency of RNAi, cytoskeleton perturbation is a rather harsh treatment that may also indirectly impair RNA silencing. We therefore hypothesized that a strategy to enhance RNAi by perturbation of anterograde transport and the resulting general accumulation and concentration of material at the ER by Brefeldin A treatment might allow addressing this question more specifically. Indeed, Brefeldin A pre-treatment (10 μg/ml) resulted in the opposite effect and accelerated and increased SSB mRNA knockdown as compared to the DMSO control (Figure 6C). Interestingly, the IC_{50} of the SSB siRNA was additionally shifted to lower concentrations, resulting in an ~10-fold higher siRNA efficiency at 24 h (Supplementary Figure S5D). Altogether, these data show that nucleation of RISC loading and mRNA slicing at the ER membrane is not qualitatively essential but physiologally important for the kinetics and efficiency of this process.

Discussion

In this work, we have demonstrated that Ago2 associates to the cytosolic side of the rER membrane, that loaded and active Ago2 is mostly membrane associated, and that the slicing product as well as mature siRISC co-sediment with the rER. Additionally, also RLC bound to double-stranded siRNA is enriched at the rER. Our data therefore strongly suggest a model where canonical RISC loading of Ago2 through Dicer and TRBP/PACT, encounter of RISC with target mRNA as well as siRNA-mediated mRNA slicing all occurs primarily at the cytosolic membrane surface of the rER (Figure 7A). Altogether these data show that the compartmentalization and thereby the nucleation of RISC loading and mRNA slicing at the ER membrane is physiologically important for the kinetics and efficiency of RNAi. While genomic analysis confirms the general textbook view that stable association and translation of mRNAs at the ER correlates well with predicted motifs for protein secretion or membrane anchoring (Diehn *et al*, 2006), it has also been shown that most mRNAs at least transiently associate with the ER during their lifecycle (Lerner *et al*, 2003; Gerst, 2008; Chen *et al*, 2011). Given the high dynamics of peripheral ER, the nucleation site of siRNA-mediated silencing being on the cytosolic side of the rER membrane seems not at all incompatible with silencing of mRNAs of soluble proteins. Rather, this localization provides the ER-bound RISCs a privileged predisposition to dynamically sample over translationally active mRNAs. As an important note, based on our data we cannot exclude that silencing would not function in other sites of the cell as well; however, from a quantitative point of view, compartmentalization of the initial steps of RNA silencing at endomembranes, and in particular at the rER is absolutely plausible given that only few molecules of active RISC per cell are sufficient to silence even relatively abundant mRNAs within <1 h upon initial cell exposure to siRNA. Such efficiency would be thermodynamically and kinetically

implausible if all partners were homogeneously distributed throughout the cytosol. As a side observation, our findings are also consistent with the site at which the hepatitis C virus (HCV) replicates using RISC components. HCV forms a replication complex in a membranous web derived from the rER, and requires both Ago2 and miR-122 for efficient replication (Jopling *et al*, 2005; Wilson *et al*, 2011).

Previous investigations have largely been focused on localization and tracing of overexpressed bulk RNAi pathway proteins, miRNA or siRNA. In this work, we show that after lipid delivery and endosomal entry of siRNA into mammalian cells, the lion's share gets cleared within a few hours and a very small fraction ($\ll$0.25–0.1%) is eventually loaded into Ago2 (Figure 7B). As the small number of active siRISC molecules per cell is masked by such a huge excess of both, non-productive siRNA and additional pools of Ago2, in this work we aimed to specifically trace functional RISCs and RNAi activity, which might explain the partially different conclusions compared to previous reports (Liu *et al*, 2005; Sen and Blau, 2005; Jagannath and Wood, 2009). In a previous study which used fluorescence cross correlation spectroscopy to also explicitely trace the minute fraction of siRNA-Ago2 complexes on the massive background of bulk Ago2 and siRNA (Ohrt *et al*, 2008), cytoplasmic siRISC showed a slow translational diffusion time either reflecting a very large complex and/or confined movement, generally supporting a (dynamic) membrane anchoring of loaded RISC. Furthermore, our findings are also fully consistent with a recent report that shows that membrane association of Ago1 in *A. thaliana* is required for miRNA activity (Brodersen *et al*, 2012).

After initial encounter and endonucleolytic cleavage of the target mRNA by Ago2 at the rER, the sliced mRNA (or silenced miRNP) may likely be taken up by P-bodies to facilitate the degradation of the mRNA. This would be consistent with the repeated detection of siRNA as well as Ago2 and particularly Ago2-GFP in P-bodies (Liu *et al*, 2005; Sen and Blau, 2005; Leung *et al*, 2006; Ohrt *et al*, 2008; Jagannath and Wood, 2009), as well as the notion that P-bodies, while clearly involved in RNAi, are rather a consequence than cause of silencing. Interestingly, life cell microscopy supports a transient and dynamic association of Ago2-GFP, which is known to be primarily P-body associated, with the ER (Supplementary Movie S1). Also, 'consumed' RISC may dissociate from the mRNP after slicing and recycle back to the rER via the Golgi, and the second minor pool of mature siRISC which we detect in the Golgi/P-body fractions might reflect either of these possible downstream steps (Figure 5C).

At least two studies have implicated membranes of the endo/lysosomal system as important sites in the RNA silencing pathways in mammalian cells and flies (Gibbings *et al*, 2009; Lee *et al*, 2009; Gibbings and Voinnet, 2010). These studies reported that GW bodies, membrane enclosed granules rich in GW182/Tnrc6, miRNAs, and Ago proteins are MVB associated. Blocking MVB turnover enhanced, whereas blocking MVB maturation inhibited miRNA-mediated target mRNA silencing, indicating that MVBs and GW bodies are functionally involved in miRNA-mediated RNA silencing. As also RISC loading was enhanced upon inhibiting MVB turnover by Hps4 knockdown (Lee *et al*, 2009), the authors argued that MVBs might also be sites of RISC disassembly, and possibly RISC loading. However, the increased levels of loaded RISC might as well be an indirect consequence of enhanced RISC disassembly upon impaired MVB turnover, which would facilitate recycling to and *de novo* loading at another site. In light of our data, it seems plausible that endo/lysosomal compartments rather play a role downstream of RISC loading. While our data show that canonical RISC loading, initial RISC-mRNA binding and slicing happen at the rER, the siRNPs or miRNPs may then likely be sorted into different effector compartments for downstream events such as mRNA degradation in P-bodies or translational silencing in MVBs and MVB-associated GW bodies, and that consumed RISC is continuously recycled back from such effector sites to the rER as the primary nucleation site of RNAi. This model not only reconciles much of the apparently controversial evidence in the literature, but most importantly may now enable the rational design of a new generation of therapeutic siRNA delivery strategies.

Materials and methods

Cell culture, transfections and plasmids

HeLa cells were grown in RPMI (Invitrogen) supplemented with 10% fetal bovine serum. For transfections, 2×10^5 or $1–2 \times 10^6$ cells were seeded into 6-well plates or 10 cm^2 dishes, respectively, and transfected the next day. siRNAs were transfected with Lipofectamine 2000 (Invitrogen) according to manufacturer's protocol. For TRBP or PACT knockdowns, HeLa cells were transfected in 10 cm^2 dishes with 25 nM siRNA, and re-transfected with 25 nM siRNA 24 h later. The cells were used for the experiments 48–96 h after the first transfection. For luciferase reporters, a 1.2-kb fragment of the HuR mRNA starting at position +1 of the 3′UTR comprising the HuR siRNA binding site (position 1186 in GenBank accession number NM001419) in either sense or antisense orientation was generated by gene synthesis and cloned into the *Xho*I and *Not*I sites of psiCHECK-2 plasmids (Promega).

Luciferase assays

In all experiments, 7000 HeLa cells/well were seeded into 96-well plates. The next day, 50 ng psi-Check2 plasmid was co-transfected with siRNA using Lipofectamine 2000 (Invitrogen) and 24 h later renilla and firefly luciferase activities were measured using the Dual Luciferase Assay System from Promega on a GloMax-Multi+ Microplate Multimode Reader (Promega) according to manufacturer's protocol.

siRNAs and antibodies

The siRNAs have the following sequences:
SSB (guide: 5′-UUACAUUAAAGUCUGUUGUUU-3′;
Passenger 5′-ACAACAGACUUUAAUGUAAUU-3′),
HuR (guide: 5′-UUAAUUAUCUAUUCCGUACTT-3′;
Passenger 5′-GUACGGAAUAGAUAAUUAATT-3′),
pGL3 (guide: 5′-UCGAAGUACUCAGCGUAAGUU-3′;
Passenger 5′-CUUACGCUGAGUACUUCGAUU-3′),
SSB(53) (guide: 5′-CCUUUGUAAUAUGAGAAUGUU;
Passenger: 5′-CAUUCUCAUAUUACAAAGGUU-3′),
GAPDH (guide: 5′-GGCCAUCCACAGUCUUCUGdGdG-3′;
Passenger: 5′- CAGAAGACUGUGGAUGGCCdTdT-3′;),
Renilla (guide: 5′-UCGAUGAACAUCUUAGGCATT-3′;
Passenger 5′-UGCCUAAGAUGUUCAUCGATT-3′),
YFP (guide: 5′-CUUGUCGGCCAUGAUAUAGAC-3′;
Passenger 5′-CUAUAUCAUGGCCGACAAGTT-3′).

TMR labelled HuR siRNA was labelled via a 5′terminal amino-C6 linker at the guide strand (Eurogentec). ON-TARGETplus SMARTpool siRNAs (Dharmacon) were used to deplete TRBP (L-017430-00) or PACT (L-006426-00).

Antibodies against Ago2 (clone 11A9 or 4G8) were from Ascenion or Wako Chemicals, respectively, antibody against Ago1 (clone 4B8) was from Ascenion. Antibodies against Hrs (ab56468), Rab5 (ab18211), tsg101 (ab83), lamp2 (ab25631), calnexin (ab22595), Dcp1a (ab47811) and TRBP (ab42018) were from Abcam, and

antibodies against calreticulin (A301-130A), RPS6 (A300-557A), PACT (A302-016A) and Dicer (A301-936A) were from Bethyl Laboratories. Antibodies against p58 (sc-66880) and GM130 (sc-16268) were from Santa Cruz; antibodies against b4-GalT1 (HPA010807) were from Atlas antibodies; and antibodies against SmB (S0698) were from Sigma. A rabbit antibody against dicer (Haase *et al*, 2005) was a kind gift from W Filipowicz.

Immune precipitations

Magnetic protein G sepharose beads (GE Healthcare) were incubated at 4°C with saturating amounts of antibody for 2 h or overnight. Unless stated differently, 15 mg anti-Ago2 antibody was coupled to 10 μl beads in a total volume of IP buffer (0.1% v/v Nonidet-P40, 100 U/ml RNasIn (Promega), 0.5 mM DTT, 20 mM Tris–HCl 7.4, 150 mM NaCl, 1 mg/ml heparin and complete EDTA-free protease inhibitor (Roche)). For the Ago2-IP in Figure 2, 22.5 mg anti-Ago2 antibody was coupled to 20 μl beads. For whole-cell extracts, cells were incubated in lysis buffer (20 mM Tris–HCl 7.4, 150 mM NaCl, 0.5% v/v NP-40, 2 mM EDTA, 1 mg/ml heparin, 2.5 mM DTT, 500 U/ml RNAsin (Promega) and Complete^{TM} EDTA-free protease inhibitor (Roche)) and centrifuged at 1000 *g* for 5 min. For sucrose gradient fractions, 200 μl from each fraction was incubated with lysis buffer. For the IP in Supplementary Figure S2F and G, 11.25 mg anti-Ago2 antibody was coupled to 10 μl beads, then 2 μM recombinant Ago2 with 5 μM 3′TMR HuR guide strand. IPs were rotated head over tail for 2–4 h at 4°C in IP buffer. Beads were washed twice with IP wash buffer (50 mM Tris–HCl 7.4, 300 mM NaCl, 5 mM $MgCl_2$, 0.05% v/v NP-40). Proteins were eluted by incubating the beads for 10 min at 70°C in SDS loading buffer. For small RNA elution, beads were incubated for 10 min at 95°C in elution buffer (6 mM TCEP (tris(2-carboxyethyl) phosphine), 1 mM HCl, 1% v/v Triton X-100). For *in vitro* slicing reactions, beads were incubated for 45 min at 37°C with 1 μM target RNA (5′-Cy3-ACCGUCUAACAACAGACUUUAAUGUAAUUGUGGAA-3′) in RLC buffer (20 mM Tris–HCl 7.4, 50 mM NaCl, 3 mM $MgCl_2$, 2 mM DTT, 0.5 mg/ml tRNA, 2 U/μl RNAsin (Promega)). Slicing products were separated on 15% denaturing polyacrylamide TBE urea gels and visualized using a Pharos FX (BioRad).

For membrane IPs with post-nuclear supernatants, cells were incubated for 18 h at 37°C with cytochalasinD (10 μM) and nocodazole (13 μM), trypsinized and washed with PBS pH 7.2 (Invitrogen), and incubated in hypotonic buffer for 10 min on ice. Cells were then lysed similar as for sucrose gradients (20 strokes, 12 μm tungsten ball). Lysates were cleared for 5 min at 500 *g*, and the supernatant was incubated with 15 μg antibody for 2.5 h at 4°C in PBS pH 7.2 supplemented with Complete EDTA-free protease inhibitor (Roche), cytochalasinD (25 μM) and nocodazole (33 μM), and respectively 0.4% v/v NP-40 for the control sample. In all reactions, 25 μl ProteinG dynabeads (Invitrogen) were blocked with 2.5% w/v bovine serum albumine (BSA) in PBS pH 7.2, and antibody–protein complexes were captured for 30 min at 4°C. Beads were washed three times with IP wash buffer (without Nonidet P-40), and proteins were eluted by incubating the beads for 5 min at room temperature with 0.4% v/v Nonidet P-40 in PBS pH 7.2. For membrane IPs out of sucrose gradients, 200 μl of the fractions was used as input, and the IP was performed with 5 μg antibody in the absence of nocodazole and cytochalasinD.

Immune blotting and RT–qPCR

Whole cell lysates corresponding to $1–2 \times 10^5$ cells per lane or aliquots of sucrose gradient fractions or IPs were heated for 10 min at 70°C and electrophoresed on 4–12% NuPage gels (Invitrogen). Proteins were transferred onto Protran nitrocellulose membranes (Whatman) using an SD Transblot system (BioRad) and incubated with primary antibodies. Immune complexes were visualized using HRP-conjugated anti-rabbit, anti-mouse, anti-goat and anti-rat antibodies (Santa Cruz) on a Biorad XRS system.

For mRNA quantifications, total RNA was isolated using the RNeasy Plus kit (Qiagen). One-Step RT–qPCRs were performed using 40 ng RNA, 1 mM dNTPs, 0.5 U Multiscribe reverse transcriptase (Applied Biosystems), 0.03 U FastStart Taq polymerase (Roche) in GeneAmp PCR buffer I (Applied Biosystems). Samples were heated to 50°C for 30 min, then 95°C for 10 min, and then cycled 40 times with 3 s at 95°C and 30 s at 50°C on a 7900HT Fast RT–qPCR System (Applied Biosystems). SSB and GAPDH mRNA were measured using Assay-on-demand reagents from Applied Biosystems (hs00427601_m1 and 4333764, respectively). For small RNA quantifications, an adapted RT–qPCR protocol from Pei *et al* (2010) was used.

Sucrose sedimentation gradients

In all experiments, 2–4 confluent 10 cm^2 dishes with HeLa cells were used for each gradient. Cells were washed with PBS pH 7.2, then incubated for 10 min at 4°C in hypotonic buffer (HB; 10 mM Tris pH 8, 10 mM KCl, 1.5 mM $MgCl_2$, 10 mM DTT, 1x complete EDTA-free protease Inhibitors (Roche), 400 U/ml RNasIn (Promega)) and then lysed with 20 strokes in a cell homogenizer (Isobiotec) using the 12-μm tungsten ball. Lysates were cleared for 5 min at 500 *g*, and the supernatant was loaded on top of a previously prepared continuous sucrose gradient. To generate the gradients, sucrose dissolved in HB was overlaid and frozen between each step, then the gradient was thawed overnight at 4°C to allow the formation of a continuous gradient. The gradient was centrifuged for 16 h at 100 000 *g* at 4°C in a Beckman Optima Max, and fractions were collected from the top.

Membrane floatation assays

Membrane floatation assays were essentially performed as described elsewhere (Tahbaz *et al*, 2004). Sucrose solutions and cell lysates were prepared as for the sucrose sedimentation gradients.

Immune cytochemistry

Immune cytochemistry was essentially performed as described elsewhere (Stalder and Muhlemann, 2009). Briefly, $0.5–1.5 \times 10^5$ HeLa cells were seeded into an μ-slide VI0.4 (Ibidi). The next day, the cells were washed with PBS, fixed for 30 min at 37°C in DSS-IF-buffer (PBS pH 7.2 containing 2 mM $MgCl_2$, 10% v/v glycerol, 0.5 mM disuccinimidyl suberate (DSS, Pierce)), and subsequently washed five times with DSS-IF-buffer without DSS and permeabilized for 20 min with PBS pH 7.2 containing 0.2% v/v Triton X-100 and 0.2 M glycine. The cells were incubated for 30 min with Signal-iT FX Signal Enhancer (Invitrogen), washed with PBS containing 0.15% w/v BSA and incubated with primary antibodies for 1 h at room temperature. The cells were then washed five times with PBS containing 0.15% BSA and incubated with primary antibodies for 1 h at room temperature and washed five times with PBS containing 0.15% BSA. Anti-rat AlexaFluor488 (Molecular Probes) and anti-rabbit or anti-mouse AlexaFluor647 (Molecular Probes) were used as secondary antibodies, images were taken on a Zeiss LSM710 confocal microscope with a 63 × Water immersion 1.2 NA objective.

Live cell imaging

HeLa cells were seeded into an 8-well μ-slide (Ibidi) and at 60% confluency transfected with 12 nM 5′TMR-labelled HuR siRNA (guide strand, Eurogentec) using Lipofectamine 2000 according to manufacturer's protocol. To stain the endosomes or lysosmes, Alexa Fluor 647-labelled transferrin (2.5 μM) or lysotracker green (10 μM, Invitrogen) was added 30 min before the images were taken. Images were acquired on a confocal LSM710 microscope with GaAsp-detector (Zeiss) with a × 100 oil 1.4 NA objective and temperature, gas and humidity control unit (Life Imaging Services) and analysed with Imaris64 (Bitplane).

5′RACE

Total RNA was isolated from the sucrose gradient fractions with Trizol LS (Invitrogen). 5′RACE was performed with the Generacer kit (Invitrogen) according to the manufacturer's protocol. The following primers were used: RT-primer and first PCR primer (5′-GGCCAGGGGTCTCTACAAAT-3′), nested reverse (5′-AGAGTTGCATCAGTTGGGAAG-3′).

Fluorescence anisotropy measurements

Binding of HuR siRNA or miR-122 to recombinant Ago2 as well as off rates were measured with anisotropy determination by 2D-FIDA as described elsewhere (Kask *et al*, 2000; Meisner *et al.*, 2004). For binding curves, 1 nM of 5′TMR-labelled miR-122 (5′TMR-UGGAGUGUGACAAUGGUGUUUG, EuroGentec) or HuR siRNA (5′-UUAAUUAUCUAUUCCGUACTT-3′) was incubated with increasing concentrations of recombinant human full-length Ago2 protein for at least 15 min at room temperature (23°C) in a buffer of PBS pH 7.2, 0.1% (w/v) Pluronic F-127 (Molecular Probes), 1 mM $MgCl_2$ and 1 mM DTT. 2D-FIDA measurements and anisotropy calculations were done as described previously (Meisner *et al*, 2004). Samples

of Ago2-loaded 5′TMR HuR siRNA before and after IP were measured under the same conditions. For off rate measurements, 1 nM of 5′TMR labelled miR-122 was incubated with hAgo2 at 2.6 μM (corresponding to 95% complex formation according to the affinity determination) for 10 min. Unlabelled competitor guide (5′phosphorylated miR-16, UAGCAGCACGUAAAUAUUGGCG, Eurogentec) was added at 10 μM and the 2D-FIDA measurement was started, whereas the exact delay time between the addition of the competitor and the start of the measurement was taken with a chronometer. All curve fits were done by non-linear regression in GraFit as described (Meisner *et al*, 2004). Off rates were fitted to a pseudo first-order mono-exponential decay, binding curves were fitted to the equation describing the anisotropy in dependence of 1:1 complex formation.

Data analysis

All data are representatives from at least two to three independent experiments. Unless stated otherwise, error bars represent standard deviations from at least three technical replicates of one representative biological experiment. Non-linear curve fitting was performed using GraFit 5.0. For absolute quantification of siRNA and siRISC molecule numbers per cell, cells used per IP were counted and related to the amount of siRNA in the whole IP, which was extrapolated from the siRNA amount in the RT–qPCR with calibration to an external synthetic siRNA standard. Based on the combined errors of all steps, the overall accuracy of this analysis lies within a factor of ca 2–3.

Supplementary data

Supplementary data are available at *The EMBO Journal* Online (http://www.embojournal.org).

Acknowledgements

We thank Julien Bethune, Witold Filipowicz and Larry Gerace for very inspiring discussions, Iwan Beuvink and the NIBR siRNA synthesis team for providing reagents, and Witold Filipowicz for providing reagents and cross reading the manuscript.

Author contributions: The study was designed by DM, NM and LSt. Life cell imaging experiments in Figure 1D and Supplementary Figure S1 were performed by WH, tools for imaging studies were generated by MH. Luciferase experiments in Figure 5F and Supplementary Figure S4 were performed by VP, luciferase plasmids were cloned by FA. The Ago2-IPs in Supplementary Figure S2F and G were performed by LS, the experiments for Supplementary Figure S2N–P were performed by LS, DT and JWi, the half-life measurements in Supplementary Figure S2H by PB. Experiments for Ago2 GFP fractionation were performed by JH, DT and AF, computational analysis of siRNAs was performed by JWe. All other experiments were performed by LSt. Experiments were performed under supervision of NM with consultance of DM and MH. NM and LSt designed the experiments and wrote the manuscript.

References

Barbato C, Ciotti MT, Serafino A, Calissano P, Cogoni C (2007) Dicer expression and localization in post-mitotic neurons. *Brain Res* **1175:** 17–27

Brodersen P, Sakvarelidze-Achard L, Schaller H, Khafif M, Schott G, Bendahmane A, Voinnet O (2012) Isoprenoid biosynthesis is required for miRNA function and affects membrane association of ARGONAUTE 1 in Arabidopsis. *Proc Natl Acad Sci USA* **109:** 1778–1783

Carthew RW, Sontheimer EJ (2009) Origins and Mechanisms of miRNAs and siRNAs. *Cell* **136:** 642–655

Chen Q, Jagannathan S, Reid DW, Zheng T, Nicchitta CV (2011) Hierarchical regulation of mRNA partitioning between the cytoplasm and the endoplasmic reticulum of mammalian cells. *Mol Biol Cell* **22:** 2646–2658

Chendrimada TP, Finn KJ, Ji X, Baillat D, Gregory RI, Liebhaber SA, Pasquinelli AE, Shiekhattar R (2007) MicroRNA silencing through RISC recruitment of eIF6. *Nature* **447:** 823–828

Chu CY, Rana TM (2006) Translation repression in human cells by microRNA-induced gene silencing requires RCK/p54. *PLoS Biol* **4:** e210

Cikaluk DE, Tahbaz N, Hendricks LC, DiMattia GE, Hansen D, Pilgrim D, Hobman TC (1999) GERp95, a membrane-associated protein that belongs to a family of proteins involved in stem cell differentiation. *Mol Biol Cell* **10:** 3357–3372

Czech B, Hannon GJ (2011) Small RNA sorting: matchmaking for Argonautes. *Nat Rev Genet* **12:** 19–31

Daniels SM, Melendez-Pena CE, Scarborough RJ, Daher A, Christensen HS, El FM, Purcell DF, Laine S, Gatignol A (2009) Characterization of the TRBP domain required for dicer interaction and function in RNA interference. *BMC Mol Biol* **10:** 38

Diehn M, Bhattacharya R, Botstein D, Brown PO (2006) Genome-scale identification of membrane-associated human mRNAs. *PLoS Genet* **2:** e11

Eckmann CR, Jantsch MF (1997) Xlrbpa, a double-stranded RNA-binding protein associated with ribosomes and heterogeneous nuclear RNPs. *J Cell Biol* **138:** 239–253

Eulalio A, Behm-Ansmant I, Izaurralde E (2007a) P bodies: at the crossroads of post-transcriptional pathways. *Nat Rev Mol Cell Biol* **8:** 9–22

Eulalio A, Behm-Ansmant I, Schweizer D, Izaurralde E (2007b) P-body formation is a consequence, not the cause, of RNA-mediated gene silencing. *Mol Cell Biol* **27:** 3970–3981

Gerst JE (2008) Message on the web: mRNA and ER co-trafficking. *Trends Cell Biol* **18:** 68–76

Gibbings D, Voinnet O (2010) Control of RNA silencing and localization by endolysosomes. *Trends Cell Biol* **20:** 491–501

Gibbings DJ, Ciaudo C, Erhardt M, Voinnet O (2009) Multivesicular bodies associate with components of miRNA effector complexes and modulate miRNA activity. *Nat Cell Biol* **11:** 1143–1149

Gregory RI, Chendrimada TP, Cooch N, Shiekhattar R (2005) Human RISC couples microRNA biogenesis and posttranscriptional gene silencing. *Cell* **123:** 631–640

Haase AD, Jaskiewicz L, Zhang H, Laine S, Sack R, Gatignol A, Filipowicz W (2005) TRBP, a regulator of cellular PKR and HIV-1 virus expression, interacts with Dicer and functions in RNA silencing. *EMBO Rep* **6:** 961–967

Huizing M, Anikster Y, Gahl WA (2000) Hermansky-Pudlak syndrome and related disorders of organelle formation. *Traffic* **1:** 823–835

Iki T, Yoshikawa M, Nishikiori M, Jaudal MC, Matsumoto-Yokoyama E, Mitsuhara I, Meshi T, Ishikawa M (2010) *In vitro* assembly of plant RNA-induced silencing complexes facilitated by molecular chaperone HSP90. *Mol Cell* **39:** 282–291

Iwasaki S, Kobayashi M, Yoda M, Sakaguchi Y, Katsuma S, Suzuki T, Tomari Y (2010) Hsc70/Hsp90 Chaperone Machinery Mediates ATP-Dependent RISC Loading of Small RNA Duplexes. *Mol Cell* **39:** 292–299

Jagannath A, Wood MJ (2009) Localization of double-stranded small interfering RNA to cytoplasmic processing bodies is Ago2 dependent and results in up-regulation of GW182 and Argonaute-2. *Mol Biol Cell* **20:** 521–529

Jakymiw A, Lian S, Eystathioy T, Li S, Satoh M, Hamel JC, Fritzler MJ, Chan EK (2005) Disruption of GW bodies impairs mammalian RNA interference. *Nat Cell Biol* **7:** 1267–1274

Janas MM, Wang B, Harris AS, Aguiar M, Shaffer JM, Subrahmanyam YV, Behlke MA, Wucherpfennig KW, Gygi SP, Gagnon E, Novina CD (2012) Alternative RISC assembly: binding and repression of microRNA-mRNA duplexes by human Ago proteins. *RNA* **18:** 2041–2055

Johnston M, Geoffroy MC, Sobala A, Hay R, Hutvagner G (2010) HSP90 protein stabilizes unloaded argonaute complexes and microscopic P-bodies in human cells. *Mol Biol Cell* **21:** 1462–1469

Jopling CL, Yi M, Lancaster AM, Lemon SM, Sarnow P (2005) Modulation of hepatitis C virus RNA abundance by a liver-specific MicroRNA. *Science* **309:** 1577–1581

Jouannet V, Moreno AB, Elmayan T, Vaucheret H, Crespi MD, Maizel A (2012) Cytoplasmic Arabidopsis AGO7 accumulates in membrane-associated siRNA bodies and is required for ta-siRNA biogenesis. *EMBO J* **31:** 1704–1713

Kanellopoulou C, Muljo SA, Kung AL, Ganesan S, Drapkin R, Jenuwein T, Livingston DM, Rajewsky K (2005) Dicer-deficient mouse embryonic stem cells are defective in differentiation and centromeric silencing. *Genes Dev* **19:** 489–501

Kask P, Palo K, Fay N, Brand L, Mets U, Ullmann D, Jungmann J, Pschorr J, Gall K (2000) Two-dimensional fluorescence intensity distribution analysis: theory and applications. *Biophys J* **78:** 1703–1713

Kawamata T, Tomari Y (2010) Making RISC. *Trends Biochem Sci* **35:** 368–376

Kok KH, Ng MH, Ching YP, Jin DY (2007) Human TRBP and PACT directly interact with each other and associate with dicer to facilitate the production of small interfering RNA. *J Biol Chem* **282:** 17649–17657

Lee YS, Pressman S, Andress AP, Kim K, White JL, Cassidy JJ, Li X, Lubell K, Lim dH, Cho IS, Nakahara K, Preall JB, Bellare P, Sontheimer EJ, Carthew RW (2009) Silencing by small RNAs is linked to endosomal trafficking. *Nat Cell Biol* **11:** 1150–1156

Lerner RS, Seiser RM, Zheng T, Lager PJ, Reedy MC, Keene JD, Nicchitta CV (2003) Partitioning and translation of mRNAs encoding soluble proteins on membrane-bound ribosomes. *RNA* **9:** 1123–1137

Leung AK, Calabrese JM, Sharp PA (2006) Quantitative analysis of Argonaute protein reveals microRNA-dependent localization to stress granules. *Proc Natl Acad Sci USA* **103:** 18125–18130

Leuschner PJ, Ameres SL, Kueng S, Martinez J (2006) Cleavage of the siRNA passenger strand during RISC assembly in human cells. *EMBO Rep* **7:** 314–320

Liu J, Carmell MA, Rivas FV, Marsden CG, Thomson JM, Song JJ, Hammond SM, Joshua-Tor L, Hannon GJ (2004) Argonaute2 is the catalytic engine of mammalian RNAi. *Science* **305:** 1437–1441

Liu J, Valencia-Sanchez MA, Hannon GJ, Parker R (2005) MicroRNA-dependent localization of targeted mRNAs to mammalian P-bodies. *Nat Cell Biol* **7:** 719–723

Liu Y, Ye X, Jiang F, Liang C, Chen D, Peng J, Kinch LN, Grishin NV, Liu Q (2009) C3PO, an endoribonuclease that promotes RNAi by facilitating RISC activation. *Science* **325:** 750–753

Lu JJ, Langer R, Chen J (2009) A novel mechanism is involved in cationic lipid-mediated functional siRNA delivery. *Mol Pharm* **6:** 763–771

MacRae IJ, Ma E, Zhou M, Robinson CV, Doudna JA (2008) *In vitro* reconstitution of the human RISC-loading complex. *Proc Natl Acad Sci USA* **105:** 512–517

Maniataki E, Mourelatos Z (2005) A human, ATP-independent, RISC assembly machine fueled by pre-miRNA. *Genes Dev* **19:** 2979–2990

Martinez J, Tuschl T (2004) RISC is a 5′ phosphomonoester-producing RNA endonuclease. *Genes Dev* **18:** 975–980

Matranga C, Tomari Y, Shin C, Bartel DP, Zamore PD (2005) Passenger-strand cleavage facilitates assembly of siRNA into Ago2-containing RNAi enzyme complexes. *Cell* **123:** 607–620

Meisner NC, Hackermuller J, Uhl V, Aszodi A, Jaritz M, Auer M (2004) mRNA openers and closers: modulating AU-rich element-controlled mRNA stability by a molecular switch in mRNA secondary structure. *Chembiochem* **5:** 1432–1447

Meister G, Landthaler M, Patkaniowska A, Dorsett Y, Teng G, Tuschl T (2004) Human Argonaute2 mediates RNA cleavage targeted by miRNAs and siRNAs. *Mol Cell* **15:** 185–197

Miyoshi K, Tsukumo H, Nagami T, Siomi H, Siomi MC (2005) Slicer function of Drosophila Argonautes and its involvement in RISC formation. *Genes Dev* **19:** 2837–2848

Miyoshi T, Takeuchi A, Siomi H, Siomi MC (2010) A direct role for Hsp90 in pre-RISC formation in Drosophila. *Nat Struct Mol Biol* **17:** 1024–1026

Noland CL, Ma E, Doudna JA (2011) siRNA repositioning for guide strand selection by human dicer complexes. *Mol Cell* **43:** 110–121

Ohrt T, Mutze J, Staroske W, Weinmann L, Hock J, Crell K, Meister G, Schwille P (2008) Fluorescence correlation spectroscopy and fluorescence cross-correlation spectroscopy reveal the cytoplasmic origination of loaded nuclear RISC *in vivo* in human cells. *Nucleic Acids Res* **36:** 6439–6449

Pare JM, Tahbaz N, Lopez-Orozco J, LaPointe P, Lasko P, Hobman TC (2009) Hsp90 regulates the function of argonaute 2 and its recruitment to stress granules and P-bodies. *Mol Biol Cell* **20:** 3273–3284

Pei Y, Hancock PJ, Zhang H, Bartz R, Cherrin C, Innocent N, Pomerantz CJ, Seitzer J, Koser ML, Abrams MT, Xu Y, Kuklin NA, Burke PA, Sachs AB, Sepp-Lorenzino L, Barnett SF (2010) Quantitative evaluation of siRNA delivery *in vivo*. *RNA* **16:** 2553–2563

Pillai RS, Bhattacharyya SN, Artus CG, Zoller T, Cougot N, Basyuk E, Bertrand E, Filipowicz W (2005) Inhibition of translational initiation by Let-7 MicroRNA in human cells. *Science* **309:** 1573–1576

Rand TA, Petersen S, Du F, Wang X (2005) Argonaute2 cleaves the anti-guide strand of siRNA during RISC activation. *Cell* **123:** 621–629

Rivas FV, Tolia NH, Song JJ, Aragon JP, Liu J, Hannon GJ, Joshua-Tor L (2005) Purified Argonaute2 and an siRNA form recombinant human RISC. *Nat Struct Mol Biol* **12:** 340–349

Rüdel S, Flatley A, Weinmann L, Kremmer E, Meister G (2008) A multifunctional human Argonaute2-specific monoclonal antibody. *RNA* **14:** 1244–1253

Sen GL, Blau HM (2005) Argonaute 2/RISC resides in sites of mammalian mRNA decay known as cytoplasmic bodies. *Nat Cell Biol* **7:** 633–636

Stalder L, Muhlemann O (2009) Processing bodies are not required for mammalian nonsense-mediated mRNA decay. *RNA* **15:** 1265–1273

Tahbaz N, Carmichael JB, Hobman TC (2001) GERp95 belongs to a family of signal-transducing proteins and requires Hsp90 activity for stability and Golgi localization. *J Biol Chem* **276:** 43294–43299

Tahbaz N, Kolb FA, Zhang H, Jaronczyk K, Filipowicz W, Hobman TC (2004) Characterization of the interactions between mammalian PAZ PIWI domain proteins and Dicer. *EMBO Rep* **5:** 189–194

Wilson JA, Zhang C, Huys A, Richardson CD (2011) Human Ago2 is required for efficient microRNA 122 regulation of hepatitis C virus RNA accumulation and translation. *J Virol* **85:** 2342–2350

Ye X, Huang N, Liu Y, Paroo Z, Huerta C, Li P, Chen S, Liu Q, Zhang H (2011) Structure of C3PO and mechanism of human RISC activation. *Nat Struct Mol Biol* **18:** 650–657

Yoda M, Kawamata T, Paroo Z, Ye X, Iwasaki S, Liu Q, Tomari Y (2010) ATP-dependent human RISC assembly pathways. *Nat Struct Mol Biol* **17:** 17–23

Zeng Y, Sankala H, Zhang X, Graves PR (2008) Phosphorylation of Argonaute 2 at serine-387 facilitates its localization to processing bodies. *Biochem J* **413:** 429–436